C. R. Physique 15 (2014) 176–189

Contents lists available at ScienceDirect

Comptes Rendus Physique

www.sciencedirect.com

Electron microscopy / Microscopie électronique

Seeing in 4D with electrons: Development of ultrafast electron microscopy at Caltech

Voir en 4D avec des électrons : développement de la microscopie électronique ultra-rapide au Caltech

J. Spencer Baskin, Ahmed H. Zewail *

Physical Biology Center for Ultrafast Science and Technology, Arthur Amos Noyes Laboratory of Chemical Physics, California Institute of Technology, Pasadena, CA 91125, United States of America

ARTICLE INFO

Article history:
Available online 8 December 2013

Keywords:
Near-field
PINEM
Atomic steps
Electron microscopy

Mots-clés :
Champ proche
PINEM
Marches atomiques
Microscopie électronique

ABSTRACT

The vision to develop 4D electron microscopy, a union of the capabilities of electron microscopy with ultrafast techniques to capture clearly defined images of the nanoscale structure of a material at each step in the course of its chemical or physical transformations, has been pursued at Caltech for the last decade. In this contribution, we will give a brief overview of the capabilities of three currently active Caltech 4D microscopy laboratories. Ongoing work is illustrated by a description of the most recent application of photon-induced near-field electron microscopy (PINEM), a field made possible only by the development of the 4D ultrafast electron microscopy (UEM). An appendix gives the various applications made so far and the historic roots of the development at Caltech.

RÉSUMÉ

Tout au long de ces dix dernières années, le Caltech a consacré un effort permanent au développement d'un projet visionnaire, à savoir la microscopie électronique à 4D, une union des possibilités de la microscopie électronique avec les techniques des temps ultra-courts afin de capturer des images claires de la structure nanométrique des matériaux au cours des différentes étapes de leur transformation. Dans cette contribution, nous présentons une brève revue des possibilités techniques des trois plates-formes de microscopie électronique 4D actuellement opérationnelles au Caltech. Parmi les travaux en cours, nous décrirons plus spécialement les résultats les plus récents obtenus en microscopie électronique photo-induite de champ proche (PINEM), un domaine rendu accessible uniquement par les progrès en microscopie électronique ultra-rapide. Nous terminerons par une revue des diverses applications réalisées à ce jour au Caltech dans le prolongement de leurs sources historiques.

* Corresponding author.
E-mail address: zewail@caltech.edu (A.H. Zewail).

1631-0705/$ – see front matter
http://dx.doi.org/10.1016/j.crhy.2013.11.002

Advances in electron microscopy described in this special issue are today providing remarkable versatility and power for detailed structural studies of the three spatial dimensions of matter down to the atomic-scale, with applications to science and technology in a wide variety of fields. The electron microscope is today an essential tool for many types of material characterization, from composition and morphology to magnetic and electronic properties. It was therefore natural that a project was conceived a decade ago to try to integrate this power of electron microscopy to elucidate the nature of static structures with the capabilities developed in our laboratory for the study of ultrafast dynamics. Ultrafast techniques in laser spectroscopy and electron diffraction in the gas phase and on surfaces, which had been the long-standing focus of our research, are ideally suited to homogeneous media, revealing the nature and timing of ensemble-averaged structural changes; a successful extension to microscopy offered the possibility of direct observation of site-specific dynamics in complex, heterogeneous samples, opening up a new world of materials and phenomena to investigation.

From the perspective of the traditional microscopy community, a need was also clear for expansion of the capabilities of microscopy into the fourth dimension; that is, for capture of images on short time scales in order to study dynamic processes and their associated transient structures. Video rate imaging with millisecond resolution and nanosecond electron pulse imaging at the micron scale had begun to show the promise of following temporal evolution of image changes; for review, see Ref. [1]. The ultimate temporal resolution for tracking changes in material structures would clearly be that of the time scale for the motion of individual atoms in chemical and physical rearrangements—that is, femtoseconds. Reaching this time scale and preserving the atomic scale potential of electron imaging would require a new approach to leap the gap of many orders of magnitude in combined temporal/spatial resolutions.

In pursuit of this vision of developing 4D electron microscopy, the Ultrafast Electron Microscopy (UEM) laboratories were constructed at Caltech, which today consist of two transmission electron microscopes, UEM-1 and UEM-2, and a scanning ultrafast electron microscope, or S-UEM. Since the first microscopy results from UEM-1, published in 2005 [2], the UEM labs have produced upwards of 40 experimental studies of an ever widening range of microscopic systems and phenomena, from phase transition dynamics in thin films, to resonant motions of nanoscale structures, to biodynamics of DNA and protein assemblies. Results of a few of these studies are displayed in Fig. 1, illustrating the wide range of materials and time scales explored. In this contribution, we will give an overview of the current capabilities of the labs and provide as an example a summary of a recent application of 4D microscopy. More comprehensive reviews of the concepts and variety of studies undertaken and envisioned may be found elsewhere [1,3–5].

1. 4D microscopy at Caltech: An overview

The basic concept of UEM is illustrated by the schematic of the UEM-2 laboratory shown in Fig. 2. At the heart of the operation in each lab is a microscope with state-of-the-art commercial imaging capabilities that has been customized to allow generation of electron packets by photoemission when a focused light pulse impinges on the cathode. A dynamic process is initiated in the microscope sample by a second synchronized light pulse, and the electron pulse probes the state of the sample at a well-defined point in time in the sample evolution, contributing to a “frame” image on the CCD detector, with time resolution determined by the pulses’ temporal characteristics only, independent of the CCD read-out time or electronic response of a video camera. To trace out the full time-course of specimen evolution, a series of measurements is conducted with changes in the electron pulse time delay with respect to the light pulse. Imaging and diffraction detection are possible in each lab, but in this contribution, the imaging capabilities will be emphasized. The characteristics of the microscope, the laser systems, and light pulses vary depending on the lab and the specific needs of individual experiments, and will be described for each lab in turn.

First, to continue discussion of Fig. 2, we note that UEM-2 is equipped for operation in either of two time-domain regimes, with each using independent light sources and time delay selection mechanisms. In femtosecond operation, labeled “single-electron mode” in the figure (see below), light pulses for cathode and specimen irradiation are generated in nonlinear crystals from a single femtosecond IR light pulse (1038 nm) with the relative delay, Δt, fixed by sending one beam through a variable optical delay line. In other words, the time resolution in this mode has no electronic response limitations at all, in contrast to the electronic delays involved in nanosecond imaging. In typical usage, the excitation light to the specimen is the green harmonic of the IR fundamental, while the pulse on the cathode is its fourth harmonic at 259 nm, though other wavelength combinations have also been used. The alternative nanosecond operation, labeled “single-pulse mode” in the figure (see below) and accessed by two flip mirrors, uses two independent lasers to produce 532 nm and 266 nm pulses with pulse timing controlled electronically. Time delays from nanoseconds to milliseconds or longer may be studied routinely in this configuration.

The femtosecond operation was achievable when the concept of “single-electron mode” was introduced. When each electron pulse consists of a single electron, the highest temporal and spatial (and energy; see below) resolutions are possible. In that case, no space-charge broadening can occur during the time of electron propagation down the microscope column, and the temporal resolution is determined by the laser pulse lengths and electron energy spread at the source, with possible contributions from lens aberrations. Single-electron spatial resolution can be equal to that of the microscope operating with a continuous electron beam., when imaging electrons are also on average widely separated in time and do not interact. In practice, single-electron operation is achieved by simply attenuating the UV laser intensity on the cathode,

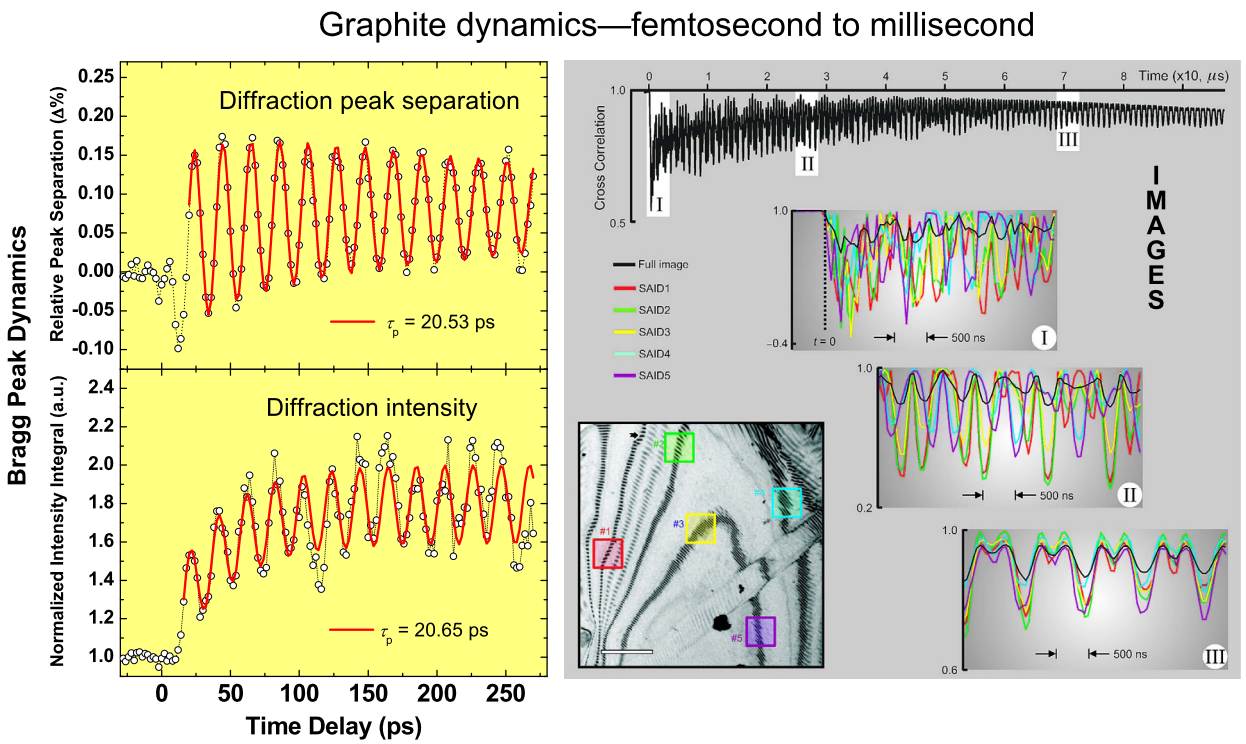

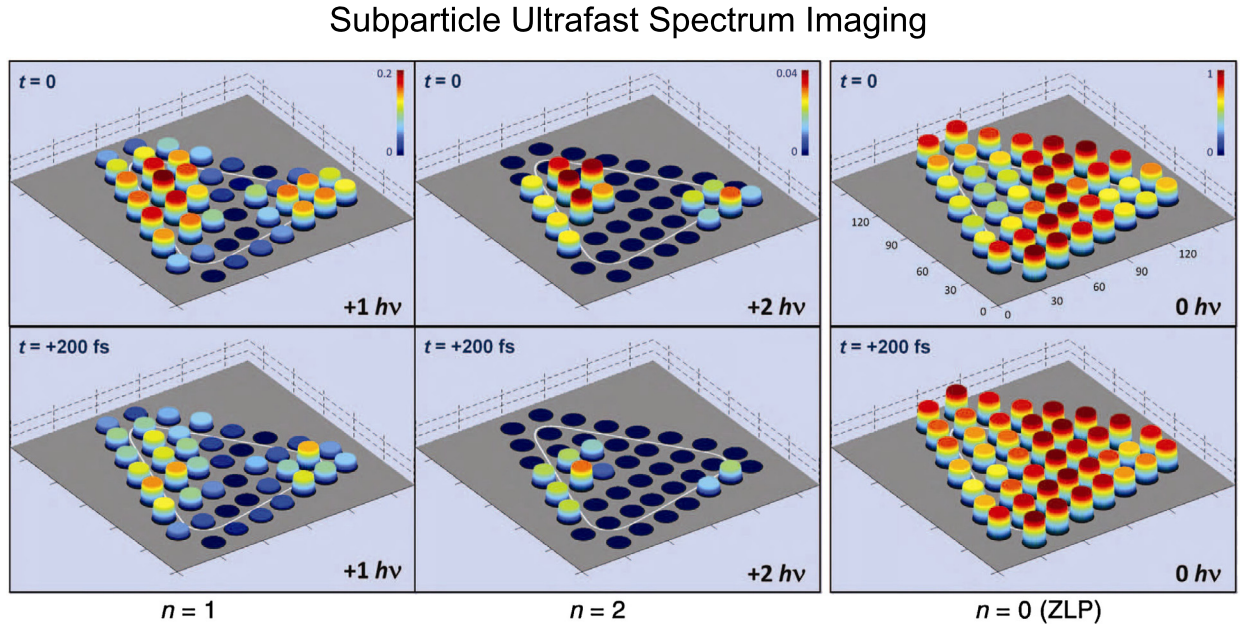

Fig. 1. (Color online.) A selection of results from the 4D microscopy labs at Caltech. Top: Graphite film resonant behaviors (adapted from [18M]). At left is a measurement of the effect on diffraction of a resonant modulation of the thickness of a 39 nm thick film. At right, transverse flexing of a micron-scale film, evolving from "chaotic" to a global resonance behavior (drumming) at long time. Middle: The femtosecond temporal and nanometer spatial variation in different orders of the spatially-resolved PINEM signal of a triangular silver nanotriangle [16]. Bottom: Biomechanical resonances of DNA nanostructures [43M] and amyloid cantilevers [47M].

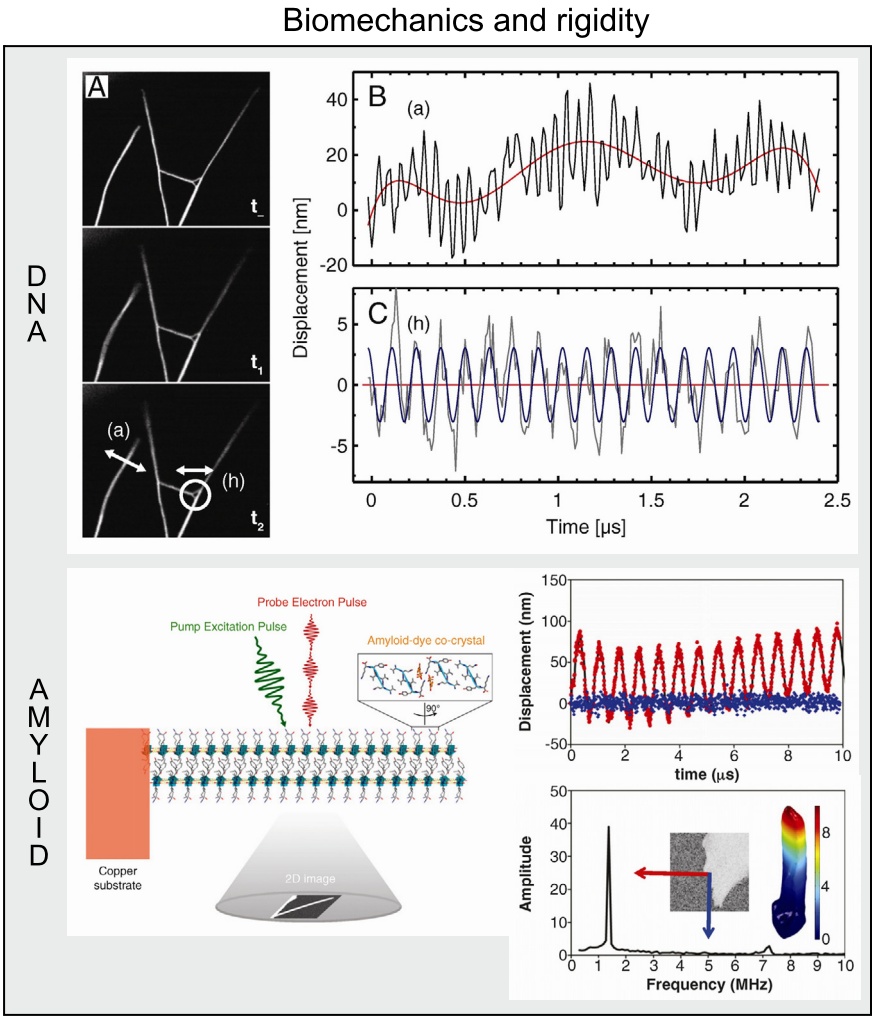

Fig. 1. (*continued*)

and the actual number of electrons in each pulse may vary while remaining below a specific, relevant, space-charge threshold.

The use of single-electron mode requires that the time between imaging pulses be longer than that of recovery of initial specimen conditions, either through reversible dynamics or change of specimen area, allowing useful images to be built up stroboscopically on the CCD detector by repeating the excitation and probe cycle under the same conditions up to millions of times. The pulse repetition rate of the femtosecond laser in UEM-2 is variable (100 kHz to 25 MHz) and can be set to allow recording of such stroboscopic images in acceptably short acquisition times, subject to the often limiting constraint of full specimen recovery between pulses. Use of the single-electron mode was a key development in UEM-1 for achieving instrument-limited resolution with ultrafast electron pulses [2]; with the 200 keV microscope in UEM-2, resolutions reaching the sub-nanometer and sub-picosecond scale have been attained.

Because the spatial volume of a nanosecond-electron-pulse is orders of magnitude larger than that of a femtosecond pulse at comparable transverse cross section, pulses containing up to 10^6 electrons are expected to traverse the electron optics of the microscope column with minimal space-charge distortions. This opens the possibility of studies of irreversible dynamics in the single-pulse mode, in which data consists of images which are each formed by collecting the electrons from one time-delayed, high-electron-count, nanosecond pulse following an excitation pulse. However, since the specimen does not recover, a new specimen area is required for each time point needed to map out the full dynamic process. Such single-pulse imaging experiments have been carried out in UEM-1 to record transient structures in an irreversible charge-transfer reaction [6].

Returning to Fig. 2, the final segments of the two optical paths for the beams to the cathode and to the specimen are shared by the two modes of operation. Each beam is focused by an external lens, then traverses a periscope for fine beam steering (not shown) attached in front of an entry window into the side of the column. A final mirror is located

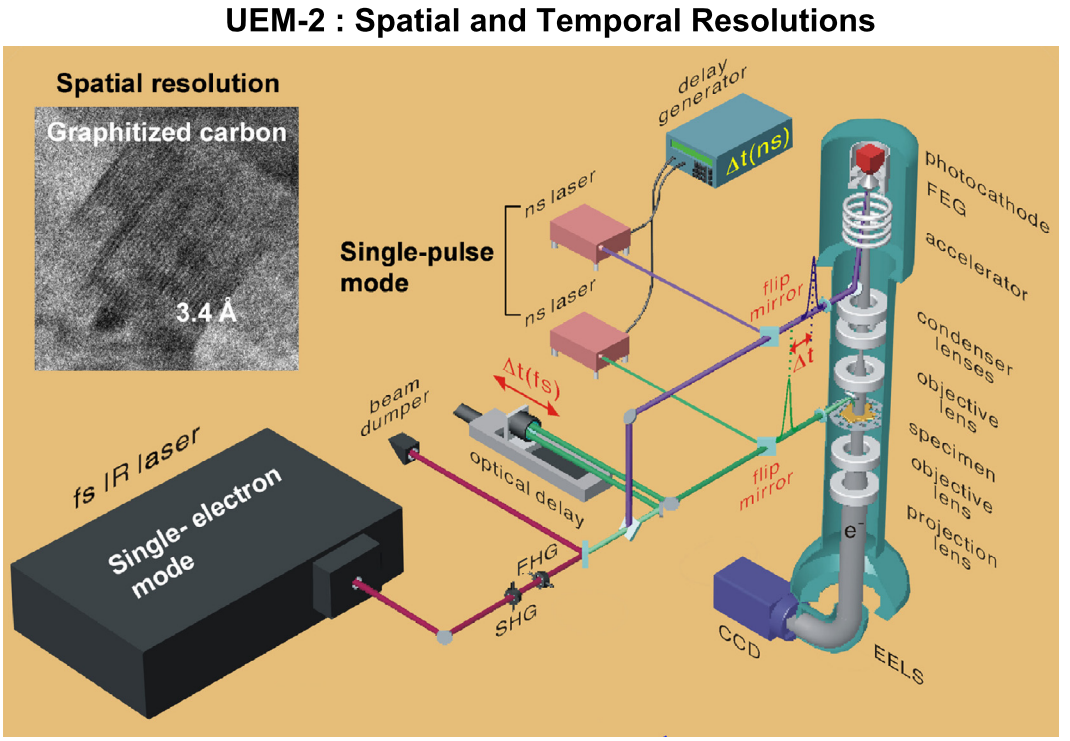

Fig. 2. (Color online.) The UEM-2 microscope at Caltech, together with a high-resolution image of a graphitized carbon film showing 3.4-Å lattice fringes. Displayed is the interface of two laser systems (fs and ns) to a modified, hybrid 200-kV TEM designed with two ports for optical access. It is straightforward to switch (by flipping two mirrors) between the laser systems to cover both the fs and ns experiments. The optical pulses are directed to the specimen to initiate a change, as well as to the photocathode to generate electron packets which probe the specimen at a well-defined time delay Δt. The time axis is defined by varying the inter-pulse delay either electronically (ns) or by an optical path length change (fs). (This figure is adapted from Ref. [18M].)

close to the electron beam path to intercept each focused beam and redirect it to its respective target, the cathode or specimen. In both UEM-1 and UEM-2, the cathode is a lanthanum hexaboride (LaB_6) flat of ∼50 μm diameter, and it can be operated both as an UEM (i.e. low temperature, photoemission) source and as a thermal emission source for conventional continuous-electron-beam microscopy. As shorthand, these two alternative operation modes are designated simply UEM and TEM. In UEM-2 the cathode is mounted in a hybrid-design field emission gun (FEG). The electron energy loss spectrometer (EELS) shown in the figure will be discussed below.

With a basic layout very similar to that shown in Fig. 2, the first generation UEM lab, UEM-1, is built around a 120 kV transmission electron microscope with a thermal electron gun design. In its current configuration, UEM-1 also operates in two time regimes [7]. In the range of picoseconds to a few nanoseconds, the arrangement is similar to that of femtosecond operation in UEM-2, but in this case with a fundamental pulse of 1064 nm at a repetition rate up to 200 kHz and 16 ps temporal width. The longer light pulses have substantially higher energy than the femtosecond pulses of UEM-2, providing more flexibility in operation. In the nanosecond and longer time regime, the time scale of study is extended while eliminating possible pump laser effects by implementing a combination of the same picosecond excitation with electronically delayed nanosecond probe pulses generated by a separate laser source. The wavelengths used for excitation and electron probe generation are typically 532 nm and 266 nm. The physical integration between microscope and laser is similar to that described for UEM-2.

Construction of the second-generation UEM laboratory in 2007 [8] allowed the addition of capabilities not available in UEM-1. Besides an increase to a 200 kV operating voltage, the UEM-2 microscope is equipped for both scanning transmission electron microscopy and EELS. The latter is essential to the studies that will be highlighted here; thus all experiments discussed in detail below were performed in UEM-2. In addition, UEM-2 has recently been equipped with an imaging apparatus designed to allow real-time tracking and control of the excitation laser beam spatial energy distribution on the specimen [Baskin and Zewail, patent pending]. A beam splitter fixed to the microscope after the steering periscope diverts a small part of the focused excitation light into a replica path where it is attenuated and monitored on a detector conjugate to the specimen plane. Thus the beam pointing and fluence at the specimen can be continually tracked and, if desired, adjusted during the course of experiments. With calibration for the optical transfer efficiency, this apparatus opens the path to precise quantitative correlation of UEM dynamics to the distribution of initiating incident light fluence.

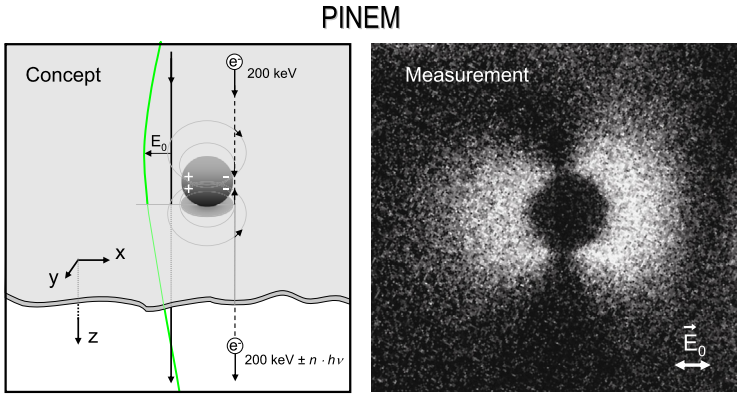

Fig. 3. (Color online.) Photon-induced near-field electron microscopy (PINEM). Left: Schematic of the concept. A femtosecond pulse of light (with electric field strength represented by the green sine wave) is overlapped in space and time with imaging electrons as they cross the specimen plane of a 4D microscope. The specimen is a nanosphere on a support film, with height much smaller than the wavelength of light. The linear polarization of the high intensity incident light field induces transient charging of the sphere surfaces leading to generation of a scatter field. A cross-section (in the *xz*-plane) of field lines of the near-field component of the transient field is represented schematically. Electrons passing near the sphere are subject to the action of this field, and work done by the *z*-component of the field can raise or lower the electron energy, in multiples of the photon energy. Right: Experimental PINEM image of a 100 nm silver nanosphere on a graphene/graphite substrate [19]. See text for details.

The latest addition to the UEM laboratories is S-UEM [9,10] for the study of dynamics at surfaces. Here, a 30 keV scanning electron microscope has been modified for pulsed operation by coupling to a single high power variable repetition rate IR femtosecond laser system of the same model described for UEM-1 femtosecond operation. The cathode is a cooled, zirconium-oxide-coated tungsten, Schottky field-emitter tip several hundred nanometer in diameter, directly irradiated from the side through a pyrometric observation window to produce photoelectron pulses. The specimen surface is likewise directly irradiated through an optical port, with the beam incident at an angle of ∼50° relative to the electron beam direction. Again, various wavelength combinations generated from the IR fundamental are possible for the two beams, with the green harmonic presently being the standard choice for both.

The microscope is equipped for secondary-electron and back-scattered-electron detection, with images built up by raster-scanning the focused spot of the incident electron beam. Because the surface-layer properties of thick or bulk specimens are studied, recovery (cooling) of reversible processes is much faster than in thin film specimens of the transmission microscope experiments. Thus high-repetition-rate (typically 12.6 MHz), stroboscopic data acquisition can be used without compromising the requirement of full recovery, with the cumulative dwell time of the electron beam for each recorded image pixel being sufficient to average thousands of laser shots. Electron beam spot sizes (pixel sizes) down to 10 nm can be used in S-UEM operation. Electron backscattering diffraction measurements can also be performed, with diffraction images recorded on a high-sensitivity digital camera. Finally, S-UEM is equipped with environmental and low-voltage-imaging capabilities to enable a broad range of investigations of surface interactions. An example is the recent study [11], using environmental S-UEM, of interfacial dynamics at a crystal surface under ambient gas pressures of hundreds of Pascal.

2. Photon Induced Near-Field Electron Microscopy

Applications made possible by the electron-energy resolution capability installed on the UEM-2 apparatus constitute a major area of activity in that lab. By combining energy resolution with femtosecond 4D microscopy, changes in electron energy in response to an incident light pulse can be mapped in space and time. For example, for excitation of an absorbing material, changes on the femtosecond to picosecond time scale in plasmon bands in EEL spectra have revealed changes in electronic structure and its effect on chemical bonding [12,13]. Another striking phenomenon observed by application of 4D energy-resolved UEM is the interaction of the electrons with the near-field components of the scattering response of polarizable nanostructures to light pulses, giving rise to electron energy loss and gain. Experiments designed to exploit this effect have been designated by the name Photo-Induced Near-field Electron Microscopy (PINEM) [14], a field which has been the subject of extensive theoretical and experimental study [15–20]. Here we describe the basic features of PINEM, using as an example the most recent results from UEM-2.

Fig. 3 provides a schematic representation of the elements involved in a PINEM experiment in UEM-2. An incident light pulse propagates down the axis of the microscope column, approximately parallel to the electron beam (*z*-axis). The specimen, here represented by a nanosphere on a support film, is discontinuous in the direction of the linear polarization of the light and of vertical dimension typically much smaller than the wavelength of light. The discontinuity in the dielectric function in the E_0 direction results in charge separation and the generation of a scatter field extending into the free space surrounding the irradiated nanostructure.

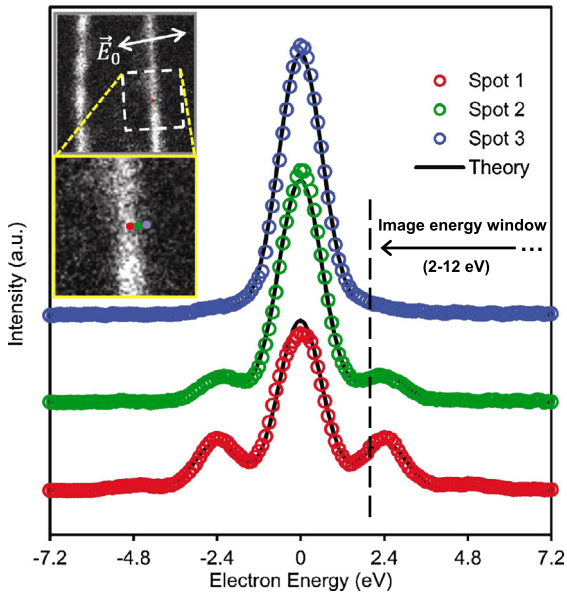

Fig. 4. (Color online.) Spatial and energy distributions of PINEM intensity at a graphene layered-step. (a) Three USI spectra give the complete electron energy distributions over 50 nm-diameter spots centered at one edge of a strip (Spot 1), and 50 (Spot 2) and 100 nm (Spot 3) away from it, respectively. The femtosecond light (fluence 4.5 mJ/cm^2) and electron pulses were coincident in time at the specimen. The energy window used for acquisition of the images in the insets is indicated. Insets: PINEM image of the area, the direction of light polarization, and the locations at which the three spectra in the main panel were recorded. The lower inset is an enlargement of the area of the dotted line box in the upper inset. The solid line fits of the three spectra are discussed in the text. (This figure is adapted from Ref. [20].)

A cross-section of the transient near-field component of such a field is represented schematically in Fig. 3, in the *xz*-plane containing the trajectory of a passing electron. In a classical picture, it is clear that the field, as represented by the arrows at four points in the figure, will act on electrons traversing this region, with work done by the *z*-component of the field along the electron trajectory. For an effectively planar specimen (i.e. height $\ll \lambda$), the *z*-components of the scatter field at any instant can be seen to be antisymmetric to the plane, so no net work would be done by a static field. The variation in the optical field during the passage of any given electron will result in unequal work contributions at distances sufficiently above and below the plane and thus lead to a net gain or loss in electron energy. It should be noted, however, that the fields near the $z = 0$ plane will be relatively ineffective, since the relativistic electron crosses this region before the light propagates a significant fraction of a wavelength. In other words, it can be said that PINEM is most sensitive to the distant field of the near field component of the scattered light [20]. The above description offers a picture of the PINEM effect that is qualitatively consistent with the detailed results of theory [15]. Quantitatively, both theory and experiment show that changes in electron energy occur only at multiples of the photon energy, $\pm n h\nu$, and that, for a given order *n*, gain and loss of energy are equally probable [14,15].

The spatial distribution of the PINEM effect reflects the strength of the *z*-component of the scatter field, with the caveat, described above, that the effect of the *z*-component increases with distance from $z = 0$. Thus, for the case of a perfect, uniform sphere, PINEM strength must diminish toward the midplane of the induced charge distribution, where the fields are horizontal, and decay with increasing distance from the particle. Timing is, of course, a critical element, as the scatter field vanishes in the absence of the incident light. A strong scatter field requires high intensity light, which can be easily achieved by femtosecond excitation, while also maintaining a low total fluence to avoid destruction of the specimen. It is thus necessary that the electron pulses be of similar duration to achieve a high probability of electron and photon interaction, and that the two pulses be carefully synchronized to arrive at the specimen simultaneously.

An example of a typical PINEM imaging experiment is shown on the right of Fig. 3, where a silver nanosphere is recorded in an energy filtered image [19]. The particle diameter is 100 nm, the light wavelength is 519 nm ($h\nu = 2.4$ eV) and the laser polarization is in the horizontal direction, as indicated. The microscope was operated in single electron mode at 400 kHz repetition rate and the energy gate selected only electrons that had gained energies of between 1 and 11 eV. The strong PINEM signal extending from each end of the particle shows where there are strong E_z components in the scatter field, as expected from the simple picture at left. The particle itself is relatively opaque to electrons, and this causes the abrupt drop in contrast at its edges. The temporal overlap of the light and electron pulses was maximized for this image; a shift of as little as 1 ps reduced the contrast dramatically.

Another component of the PINEM methodology is the recording of energy spectra, such as those displayed in Fig. 4 from the most recent PINEM study [20]. While imaging is ideal for visualizing the spatial distribution of signal sources, it can't be employed to deduce the absolute cross-sections of the energy gain process because the zero-loss peak (ZLP) of the electron beam is not recorded. In contrast, a spectrum maps the energy distribution of all incident electrons, thus providing complete knowledge about the probabilities of gain and loss. When a spectrum is formed by integrating all electrons crossing an inhomogeneous specimen region, where there may be numerous diverse scattering nanostructures contributing to the gain and loss peaks, only average spatial information is obtained about the area probed.

While not giving detailed information about the scattering fields of the specimen, this type of generic PINEM measurement can be extremely useful in the characterization of the electron beam properties. For example, tracking the variation of such a spectrum with time delay scanning is the common method employed in UEM-2 to precisely determine the time zero for non-PINEM dynamic measurements with the 4D apparatus; that is, the point on the delay axis when excitation and probe pulses arrive at the specimen simultaneously. Time zero must be routinely checked since it may change when any modification is made either to an optical element between laser and microscope, or to a microscope lens setting. The latter may cause small fractional changes in the 4 ns electron transit time from cathode to specimen, but these can be significant for the dynamics under study.

Going a step further, PINEM spectrum measurements have also been used to study in detail the time and energy characteristics of the electron pulses at the specimen plane of the microscope [17]. While generated by the light pulse at the microscope cathode, even in the single electron limit the electron pulse carries an energy distribution based on the relationship of the photon energy of the exciting pulse and the work function of the cathode. Since the higher energy electrons will, on average, travel faster to the specimen, a time/energy correlation (chirp) in the electron packets is expected to be present at that point of interaction with the light pulse. As the electron count in a packet is increased, space-charge induced broadening will intensify this effect, pushing the leading electrons ahead even faster, and retarding those at the rear of the packet.

Understanding such properties and characterizing the results of strategies designed to reduce pulse widths is an essential task in the quest for improved time resolution. A detailed experimental study [17] carried out in UEM-2 was able to quantify the chirp and its dependence on electron count by using PINEM as a temporal filter, with gating determined by the passage of the shorter exciting light pulse. In scanning the light pulse in time, not only does the PINEM signal rise and fall, revealing the electron pulse's overall temporal length, but the energies of the PINEM peaks (and of the resulting hole in the ZLP) shift, reflecting the energy of those electrons in the corresponding temporal slice of the total electron beam. The possible application of this gating property of PINEM to achieve enhanced time resolution in 4D microscopy have been examined in a separate study [21].

When PINEM is used as a probe of the scattering response of a specimen rather than of the electron pulse, maximum information is desired about the spatial distribution and strength of the PINEM signal. In this case, the electron pulses can be focused to a nanoscale spot and scanned across the area of interest, acquiring a full energy spectrum at each position. This process is referred to as Ultrafast Spectrum Imaging (USI), which was first demonstrated in a study of light scattering by a triangular plate nanostructure (see Fig. 1) and a copper grid bar, in which the spatial characteristics of different PINEM gain orders were mapped at the nanometer scale [16]. The three spectra in Fig. 4 are of the USI type, with the corresponding positions of measurement (50 nm spots) marked on the PINEM image insets in the figure. The excitation polarization direction is as shown. The energy window selected to produce the images is in turn indicated on the spectra. The solid lines are theoretical fits of the data, as discussed below.

While PINEM experiments have been performed on a wide range of different geometries, including spheres, cylinders, triangular blocks, nanoparticles with irregular shapes, and dimers and clusters of nanoparticles, the specimen in Fig. 4 is of a type that had not been studied previously by PINEM. It consists of a strip of multi-layer graphene lying on a substrate of the same material, with each having a thickness of only several atomic layers. The observations and the theoretical basis for the high signal strength from such a thin specimen have been reported recently [20] and a summary of the results is presented here.

For these measurements, specific experimental conditions were as follows. Single-electron conditions gave a full-width-at-half-maxima (FWHM) of the electron ZLP of $\sim$1.4 eV and a corresponding electron pulse temporal width of $\sim$500 fs at the specimen. The thicknesses of the strip and substrate in Fig. 4 were determined by the characteristics of the inelastic plasmon-loss signal in the static EELS [22,23], to be $\sim$4.5 nm and $\sim$1.5 nm ($\sim$13 and 4 atomic layers) respectively. The strip width was $\sim$1000 nm and its visible length $\sim$5 μ, with the underlying substrate extending across the 6 μm × 6 μm openings in a supporting copper grid. The fluence of the excitation laser ($\lambda = 519$ nm) on the specimen was 4.5 mJ/cm^2. The laser intensity was uniform over an area much wider than the opening in the supporting grid.

The three USI spectra of Fig. 4 give the complete electron energy distributions at points on one strip boundary, and 50 and 100 nm away from it. Note that the amplitude of the gain and loss peaks in each spectrum correlates with the PINEM intensity at the corresponding image location in the inset. The excitation light polarization is nearly perpendicular to the strip axis, and the PINEM signal is localized to the vicinity of the strip edge were the light scatters due to the discontinuity

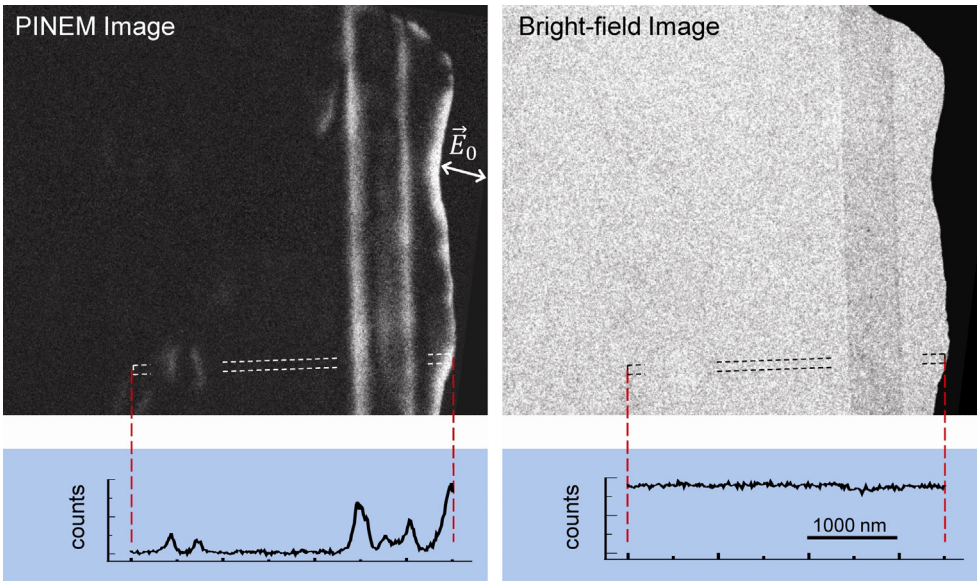

Fig. 5. (Color online.) Comparison of PINEM data and TEM bright-field data for the same area [20]. Top: Images. The graphite specimen is bounded on the right by a copper grid bar. The dotted line boxes indicate the image area from which the profiles below were extracted Bottom: Average image intensity profiles of the boxed area in the images. Intensities were averaged over the 10-pixel width of the boxes. The scale bar at lower right applies to the entire figure.

in the dielectric function in the direction of the light polarization This result is qualitatively consistent with the picture of charge accumulation and induced fields acting upon the passing electrons.

As a further confirmation of the sensitivity of PINEM to atomic scale steps, and to illustrate the large advantage in contrast relative to bright field imaging, data are presented in Fig. 5 from another grid of the same specimen, including a different layered strip 590 nm in width. In the top panels two images of the same area are compared. On the left is a standard PINEM image, with the direction of the exciting laser polarization as shown; a TEM bright-field image is displayed on the right, with its contrast stretched by a factor of two. A copper grid bar is at the right edge of the substrate. At the bottom of Fig. 5 are cross-sectional intensity profiles extracted from the same region in the two images given above, and indicated by the boxed areas in the images.

Although the graphite strip is readily visible in the TEM image, it is seen in the corresponding profile that its relative image contrast differs from the substrate by only ∼5%. On the other hand, the PINEM intensity at the strip edges is a factor of 20 to 30 times as high as the residual background intensity from the flat substrate surface, representing a contrast enhancement of at least a factor of 400. A similar comparison between PINEM and bright-field imaging for the strip of Fig. 4, shows contrast enhancement of over 1000, boosted by the lower background in the PINEM. True background in PINEM, from areas free of scatter fields, is sensitive to the width of the ZLP and the placement of the energy window.

In addition to this dramatic contrast enhancement at the strip edges in Fig. 5, it is noteworthy that other features are clearly revealed in the PINEM image that are far from evident in the TEM image. For example, the left end of each profile in Fig. 5 extends across a region that is very easily identified in the PINEM image as a discontinuity in the substrate uniformity by the two strong edge signals, with signal over background ratios greater than 8. This area (indicated by a gap in the profile box) in the bright-field image shows up with a barely discernible (∼1%) increase in contrast brightness above the background. The contrast enhancement through the use of PINEM is therefore estimated to be a factor of 800 or more. From the *increase* in TEM brightness, and the relative TEM contrast with respect to the strips in Figs. 4 and 5, it may be concluded that the steps revealed here so clearly by PINEM are the edges of a pit, or possibly a hole, in the substrate of 2 nm or less in height. The substantial PINEM contrast in this example, indicates that smaller steps, down to the sub-nanometer scale, would be detectable as well.

For a quantitative understanding of the strong PINEM response of the strip it was necessary to go beyond the previously established theory for spheres and cylinders and examine the PINEM dependence on structures with cross-sections of high aspect ratio. In this effort, an approximate analytical result for a strip with finite and independent width and height, and infinite length was derived [20]. In brief, the object was divided into a sum of infinitesimally small square beams which were then approximated as infinite circular cylinders of an equal cross-sectional area. The induced polarizations of individual cylinders were determined by the incident light and scattering from the other cylindrical elements. The total scattering field was then obtained by summing contributions from all the elements. The field integral, which represents the work

performed by the scattering field on a passing electron, was evaluated as detailed in Ref. [15]. The PINEM signal intensity varies approximately as the square of this field integral in the weak interaction limit [15].

The electric polarization inside the strip is assumed to be uniform and is given by that of an infinite elliptical cylinder of dimensions w and h. The polarization of an elliptical cylinder of high aspect ratio stretched in the direction of the applied field, is enhanced by a factor of $(1+\varepsilon)/2$ over a circular cylinder, where ε is the dielectric constant of the material. Considering only the near-field components of individual contributions, the analytical approximation predicted that for a narrow strip in the Rayleigh limit ($w \ll \lambda/2\pi$), the maximum magnitude of the field integral for a fixed aspect ratio is linearly proportional to the cross sectional area ($w \cdot h$), but for a wide strip, the width dependence saturates around $\lambda/2\pi \cdot v_e/c$ (where v_e is the electron velocity), which is 57 nm for our excitation wavelength and electron energy. The numerical calculations, including far-field contributions, showed that saturation occurred at a greater width of ∼100 nm. These results provided the basis for an estimate of the enhancement of PINEM signal amplitude of a wide strip over that of a cylinder, with both being of graphite ($|\varepsilon| \sim 10$) and both 4 nm in height. A total enhancement of ∼125 was predicted for the field integral, and therefore a 15,000-fold increase is expected in the PINEM signal at the edge of the strip vs. that at the edge of the cylinder of the same height.

Even though the elliptical approximation of a strip allows us to understand qualitatively the strength of PINEM, a strip without a substrate does not accurately represent our experimental conditions. For a quantitative comparison, the effect of the infinite substrate of a similar thickness was included with the aid of numerical simulations, which also validated the approximations used in the analytical treatment [20]. In the simulations, the polarization inside a material of arbitrary shape was obtained by solving the matrix representing the scattering interaction with an incident wave using the discrete dipole approximation, DDA. It is the results of these simulations that are plotted against the three experimental USI spectra in Fig. 4. In order to achieve good agreement in signal amplitude between the experiment and simulation, the laser intensity used in the simulation was scaled by a factor of 1.64 from that measured during the experiment. The shapes of the calculated curves were not sensitive to the assumed excitation fluence.

With regard to the slight discrepancy in the intensity response of theory and experiment, it should be noted that, while the simulations were made for a uniform planar specimen of infinite length in the y-direction, resulting in a signal with no y-dependence, the experimental PINEM contrast along the strip edges in Figs. 4 and 5 varies by at least a factor of two, presumably due to non-uniformity of the strips and substrates and effects associated with the finite lengths of the strips. It is hoped that control for these factors in experiment and theory will bring an even closer agreement, but it is already clear that the theory reproduces quite well the strong PINEM response of thin sheet specimens.

3. Conclusion

We have described here the three different implementations of 4D ultrafast electron microscopy at Caltech, providing a range of unique and complementary capabilities, reaching toward the ultimate goal of atomic scale imaging in space and time. While the instrumentation for dynamic imaging studies in UEM-1 and S-UEM have been summarized, a prime focus has been on the PINEM technique, which is enabled by 4D microscopy with electron energy resolution. The power of PINEM to probe and visualize the presence of ephemeral optical scattering fields around nanostructures has a range of possible applications, from use as a probe of fields in photonics or catalysis, to energy and time filtering in UEM, to high contrast imaging of low atomic number materials, such as carbon-based strips or cells. These last materials are weak elastic scatterers, making it a real challenge to obtain high contrast in bright-field transmission electron microscopy. As shown by the example of the study of nanoscale graphene layered-steps [20] used here to illustrate PINEM studies in UEM-2, high-contrast imaging of low atomic number materials is clearly possible by means of the PINEM technique down at least to the single nanometer scale.

A listing of all UEM studies reported thus far from our three microscopy labs is compiled in Appendix A, along with papers from the ultrafast electron diffraction (UED) and crystallography (UEC) labs at Caltech. In an accompanying figure (Fig. 6), the subjects of the UEM studies are shown rising chronologically as a structure built on the foundation of the precedent-setting works of UED and UEC. The scope of applications is wide-ranging, and we anticipate continued explorations, from materials sciences, to biological materials, to the development of new variant techniques, beyond the ones mentioned here and shown in the figure.

Acknowledgements

This work was supported by the National Science Foundation (DMR-0964886) and the Air Force Office of Scientific Research (FA9550-11-1-0055) in the Gordon and Betty Moore Center for Physical Biology at the California Institute of Technology. We wish to thank all who made this research possible; their efforts are highlighted by the publications given here. One of us (AHZ) is especially grateful to Sir John M. Thomas for his genuine interest in the development of this field since its inception, and his brilliantly-written commentary [24–29] during the evolution of UED, UEC, and UEM.

Appendix A. Development and range of applications of 4D UEM

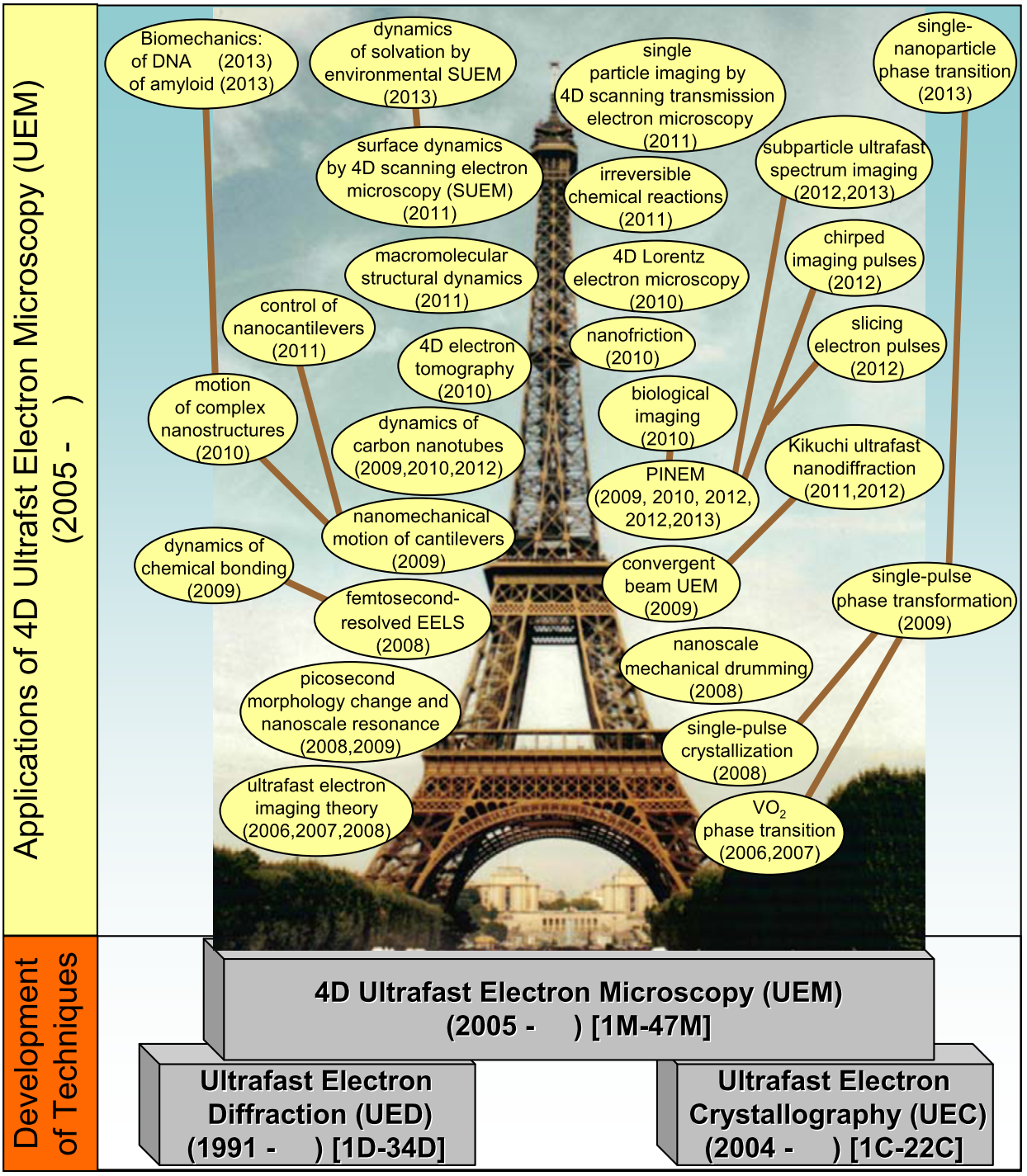

Fig. 6. (Color online.) Representation of the development and range of applications of 4D UEM. Citations to the appended complete list of publications from UED, UEC, and UEM (see below) are indicated on their respective blocks at bottom. (The newest application, that of 4D cryo-electron microscopy of biological specimens [48M] is not included in the figure.)

References

[1] A.H. Zewail, Four dimensional electron microscopy, Science 328 (2010) 187–193.
[2] V.A. Lobastov, R. Srinivasan, A.H. Zewail, Proc. Natl. Acad. Sci. USA 102 (2004) 7069–7073.

[3] D.J. Flannigan, A.H. Zewail, 4D electron microscopy: Principles and applications, Acc. Chem. Res. 45 (2012) 1828–1839.
[4] A.H. Zewail, J.M. Thomas, 4D electron microscopy, Imperial College Press, London, 2010.
[5] A.H. Zewail, Filming the invisible in 4-D, Sci. Am. 303 (2010) 74–81.
[6] S.T. Park, D.J. Flannigan, A.H. Zewail, Irreversible chemical reactions visualized in space and time with 4D electron microscopy, J. Am. Chem. Soc. 133 (2011) 1730–1733.
[7] S.T. Park, D.J. Flannigan, A.H. Zewail, 4D electron microscopy visualization of anisotropic atomic motions in carbon nanotubes, J. Am. Chem. Soc. 134 (2012) 9146–9149.
[8] H.S. Park, et al., Atomic-scale imaging in real and energy space developed in ultrafast electron microscopy, Nano Lett. 7 (2007) 2545–2551.
[9] D.-S. Yang, O.F. Mohammed, A.H. Zewail, Scanning ultrafast electron microscopy, Proc. Natl. Acad. Sci. USA 107 (2010) 14993–14998.
[10] O.F. Mohammed, D.-S. Yang, S.K. Pal, A.H. Zewail, 4D scanning ultrafast electron microscopy: Visualization of materials surface dynamics, J. Am. Chem. Soc. 133 (2011) 7708–7711.
[11] D.-S. Yang, O.F. Mohammed, A.H. Zewail, Environmental scanning ultrafast electron microscopy: Structural dynamics of solvation at interfaces, Angew. Chem., Int. Ed. 52 (2013) 2897–2901.
[12] F. Carbone, et al., EELS femtosecond resolved in 4D ultrafast electron microscopy, Chem. Phys. Lett. 468 (2009) 107–111.
[13] F. Carbone, O.H. Kwon, A.H. Zewail, Dynamics of chemical bonding mapped by energy-resolved 4D electron microscopy, Science 325 (2009) 181–184.
[14] B. Barwick, D.J. Flannigan, A.H. Zewail, Photon-induced near-field electron microscopy, Nature 462 (2009) 902–906.
[15] S.T. Park, M.M. Lin, A.H. Zewail, Photon-induced near-field electron microscopy (PINEM): Theoretical and experimental, New J. Phys. 12 (2010) 123028.
[16] A. Yurtsever, R.M. van der Veen, A.H. Zewail, Subparticle ultrafast spectrum imaging in 4D electron microscopy, Science 335 (2012) 59–64.
[17] S.T. Park, O.H. Kwon, A.H. Zewail, Chirped imaging pulses in four-dimensional electron microscopy: femtosecond pulsed hole burning, New J. Phys. 14 (2012) 053046.
[18] A. Yurtsever, A.H. Zewail, Direct visualization of near-fields in nanoplasmonics and nanophotonics, Nano Lett. 12 (2012) 3334–3338.
[19] A. Yurtsever, J.S. Baskin, A.H. Zewail, Entangled nanoparticles: Discovery by visualization in 4D electron microscopy, Nano Lett. 12 (2012) 5027–5032.
[20] S.T. Park, A. Yurtsever, J.S. Baskin, A.H. Zewail, Graphene-layered steps and their fields visualized by 4D electron microscopy, Proc. Natl. Acad. Sci. USA 110 (2013) 9277–9282.
[21] S.T. Park, A.H. Zewail, Enhancing image contrast and slicing electron pulses in 4D near-field electron microscopy, Chem. Phys. Lett. 521 (2012) 1–6.
[22] R.F. Egerton, Electron Energy-Loss Spectroscopy in the Electron Microscope, 2nd ed., Plenum Press, New York, 1996.
[23] T. Eberlein, et al., Plasmon spectroscopy of free-standing graphene films, Phys. Rev. B 77 (2008) 233406.
[24] J.M. Thomas, Femtosecond diffraction, Nature 351 (1991) 694–695.
[25] J.M. Thomas, Ultrafast electron crystallography: The dawn of a new era, Angew. Chem., Int. Ed. Engl. 43 (2004) 2606–2610.
[26] K.D.M. Harris, J.M. Thomas, Prospects for exploiting 4D ultrafast electron microscopy in solid-state organic and biological chemistry, Cryst. Growth Des. 5 (2005) 2124–2130.
[27] J.M. Thomas, A revolution in electron microscopy, Angew. Chem., Int. Ed. Engl. 44 (2005) 5563–5566.
[28] J.M. Thomas, in: A.H. Zewail (Ed.), Physical Biology: From Atoms to Medicine, Imperial College Press, London, 2008, pp. 51–113.
[29] J.M. Thomas, The renaissance and promise of electron energy-loss spectroscopy, Angew. Chem., Int. Ed. Engl. 48 (2009) 8824–8826.

Research papers of 4D ultrafast electron techniques[1]

Ultrafast Electron Diffraction (UED)

[1D] J.C. Williamson, A.H. Zewail, Structural femtochemistry: Experimental methodology, Proc. Natl. Acad. Sci. USA 88 (1991) 5021–5025.
[2D] J.C. Williamson, M. Dantus, S.B. Kim, A.H. Zewail, Ultrafast diffraction and molecular structure, Chem. Phys. Lett. 196 (1992) 529–534.
[3D] J.C. Williamson, A.H. Zewail, Ultrafast electron diffraction: Velocity mismatch and temporal resolution in cross-beam experiments, Chem. Phys. Lett. 209 (1993) 10–16.
[4D] J.C. Williamson, A.H. Zewail, Ultrafast electron diffraction. 4. Molecular structures and coherent dynamics, J. Phys. Chem. 98 (1994) 2766–2781.
[5D] M. Dantus, S.B. Kim, J.C. Williamson, A.H. Zewail, Ultrafast electron diffraction. 5. Experimental time resolution and applications, J. Phys. Chem. 98 (1994) 2782–2796.
[6D] J.C. Williamson, J. Cao, H. Ihee, H. Frey, A.H. Zewail, Clocking transient chemical changes by ultrafast electron diffraction, Nature 386 (1997) 159–162.
[7D] H. Ihee, J. Cao, A.H. Zewail, Ultrafast electron diffraction: Structures in dissociation dynamics of $Fe(CO)_5$, Chem. Phys. Lett. 281 (1997) 10–19.
[8D] J. Cao, H. Ihee, A.H. Zewail, Ultrafast electron diffraction: Determination of radical structure with picosecond time resolution, Chem. Phys. Lett. 290 (1998) 1–8.
[9D] J. Cao, H. Ihee, A.H. Zewail, Ultrafast electron diffraction and direct observation of transient structures in a chemical reaction, Proc. Natl. Acad. Sci. USA 96 (1999) 338–342.
[10D] H. Ihee, V.A. Lobastov, U.M. Gomez, B.M. Goodson, R. Srinivasan, C.-Y. Ruan, A.H. Zewail, Direct imaging of transient molecular structures with ultrafast diffraction, Science 291 (2001) 458–462.
[11D] H. Ihee, J. Cao, A.H. Zewail, Ultrafast electron diffraction of transient $Fe(CO)_4$: Determination of molecular structure and reaction pathway, Angew. Chem., Int. Ed. Engl. 40 (2001) 1532–1536.
[12D] H. Ihee, J. Kua, W.A. Goddard III, A.H. Zewail, CF_2XCF_2X and $CF_2XCF_2\bullet$ radicals (X = Cl, Br, I): Ab initio and DFT studies and comparison with experiments, J. Phys. Chem. A 105 (2001) 3623–3632.
[13D] C.-Y. Ruan, V.A. Lobastov, R. Srinivasan, B.M. Goodson, H. Ihee, A.H. Zewail, Ultrafast diffraction and structural dynamics: The nature of complex molecules far from equilibrium, Proc. Natl. Acad. Sci. USA 98 (2001) 7117–7122.
[14D] V.A. Lobastov, R. Srinivasan, B.M. Goodson, C.-Y. Ruan, J.S. Feenstra, A.H. Zewail, Ultrafast diffraction of transient molecular structures in radiationless transitions, J. Phys. Chem. A 105 (2001) 11159–11164.
[15D] H. Ihee, B.M. Goodson, R. Srinivasan, V.A. Lobastov, A.H. Zewail, Ultrafast electron diffraction and structural dynamics: Transient intermediates in the elimination reaction of $C_2F_4I_2$, J. Phys. Chem. A 106 (2002) 4087–4103.
[16D] H. Ihee, J.S. Feenstra, J. Cao, A.H. Zewail, Ultrafast electron diffraction of transient cyclopentadienyl radical: A dynamic pseudorotory structure, Chem. Phys. Lett. 353 (2002) 325–334.
[17D] B.M. Goodson, et al., Ultrafast electron diffraction: Complex landscapes of molecular structures in thermal and light-mediated reactions, Chem. Phys. Lett. 374 (2003) 417–424.
[18D] R. Srinivasan, et al., Direct determination of hydrogen-bonded structures in resonant and tautomeric reactions using ultrafast electron diffraction, J. Am. Chem. Soc. 126 (2004) 2266–2267.

[1] In the following list, publications are labeled to indicate diffraction (D), crystallography (C), and microscopy (M).

[19D] S. Xu, et al., Ultrafast electron diffraction: Structural dynamics of the elimination reaction of acetylacetone, J. Phys. Chem. A 108 (2004) 6650–6655.
[20D] R. Srinivasan, et al., Dark structures in molecular radiationless transitions determined by ultrafast diffraction, Science 307 (2005) 558–563.
[21D] J.S. Baskin, A.H. Zewail, Ultrafast electron diffraction: Oriented molecular structures in space and time, Chem. Phys. Chem. 6 (2005) 2261–2276.
[22D] J.S. Feenstra, S.T. Park, A.H. Zewail, Excited state molecular structures and reactions directly determined by ultrafast electron diffraction, J. Chem. Phys. 123 (2005) 221104.
[23D] S. Habershon, A.H. Zewail, Determining molecular structures and conformations directly from electron diffraction using a genetic algorithm, Chem. Phys. Chem. 7 (2006) 353–362.
[24D] M.M. Lin, D. Shorokov, A.H. Zewail, Helix-to-coil transitions in proteins: Helicity resonance in ultrafast electron diffraction, Chem. Phys. Lett. 420 (2006) 1–7.
[25D] S.T. Park, J.S. Feenstra, A.H. Zewail, Ultrafast electron diffraction: Excited state structures and chemistries of aromatic carbonyls, J. Chem. Phys. 124 (2006) 174707.
[26D] J.S. Baskin, A.H. Zewail, Oriented ensembles in ultrafast electron diffraction, Chem. Phys. Chem. 7 (2006) 1562–1574.
[27D] Y. He, et al., Ultrafast electron diffraction: Structural dynamics of molecular rearrangement in the NO release from nitrobenzene, Asian J. Chem. 1–2 (2006) 56–63.
[28D] S.T. Park, et al., Ultrafast electron diffraction reveals dark structures of the biological chromophore indole, Angew. Chem., Int. Ed. Engl. 47 (2008) 9496–9499.
[29D] A. Gahlmann, S.T. Park, A.H. Zewail, Structure of isolated biomolecules by electron diffraction – Laser desorption: Uracil and guanine, J. Am. Chem. Soc. 131 (2009) 2806–2808.
[30D] M.M. Lin, D. Shorokov, A.H. Zewail, Conformations and coherences in structure determination by ultrafast electron diffraction, J. Phys. Chem. A 113 (2009) 4075–4093.
[31D] M.M. Lin, D. Shorokov, A.H. Zewail, Structural ultrafast dynamics of macromolecules: Diffraction of free DNA and effect of hydration, Phys. Chem. Chem. Phys. 11 (2009) 10619–10632.
[32D] A. Gahlmann, I.-R. Lee, A.H. Zewail, Direct structural determination of conformations of photoswitchable molecules by laser desorption – electron diffraction, Angew. Chem., Int. Ed. Engl. 49 (2010) 6524–6527.
[33D] M.M. Lin, D. Shorokov, A.H. Zewail, Structural dynamics of free proteins in diffraction, J. Am. Chem. Soc. 133 (2011) 17072–17086.
[34D] I.-R. Lee, A. Gahlmann, A.H. Zewail, Structural dynamics of free amino acids in diffraction, Angew. Chem., Int. Ed. Engl. 51 (2012) 99–102.

Ultrafast Electron Crystallography (UEC)

[1C] C.-Y. Ruan, F. Vigliotti, V.A. Lobastov, S. Chen, A.H. Zewail, Ultrafast electron crystallography: Transient structures of molecules, surfaces, and phase transitions, Proc. Natl. Acad. Sci. USA 101 (2004) 1123–1128.
[2C] C.-Y. Ruan, V.A. Lobastov, F. Vigliotti, S. Chen, A.H. Zewail, Ultrafast electron crystallography of interfacial water, Science 304 (2004) 80–84.
[3C] F. Vigliotti, S. Chen, C.-Y. Ruan, V.A. Lobastov, A.H. Zewail, Ultrafast electron crystallography of surface structural dynamics with atomic-scale resolution, Angew. Chem., Int. Ed. Engl. 43 (2004) 2705–2709.
[4C] C.-Y. Ruan, D.-S. Yang, A.H. Zewail, Structures and dynamics of self-assembled surface monolayers observed by ultrafast electron crystallography, J. Am. Chem. Soc. 126 (2004) 12799.
[5C] S. Chen, M.T. Seidel, A.H. Zewail, Atomic-scale dynamical structures of fatty acid bilayers observed by ultrafast electron crystallography, Proc. Natl. Acad. Sci. USA 102 (2005) 8854–8859.
[6C] S. Chen, M.T. Seidel, A.H. Zewail, Ultrafast electron crystallography of phospholipids, Angew. Chem., Int. Ed. Engl. 45 (2006) 5154–5158.
[7C] N. Gedik, D.-S. Yang, G. Logvenov, I. Bozovic, A.H. Zewail, Nonequilibrium phase transitions in cuprates observed by ultrafast electron crystallography, Science 316 (2007) 425–429.
[8C] D.-S. Yang, N. Gedik, A.H. Zewail, Ultrafast electron crystallography I. Nonequilibrium dynamics of nanometer-scale structures, J. Phys. Chem. C 111 (2007) 4889–4919.
[9C] M.T. Seidel, S. Chen, A.H. Zewail, Ultrafast electron crystallography II. Surface adsorbates of crystalline fatty acids and phospholipids, J. Phys. Chem. C 111 (2007) 4920–4938.
[10C] J. Tang, D.-S. Yang, A.H. Zewail, Ultrafast electron crystallography III. Theoretical modeling of structural dynamics, J. Phys. Chem. C 111 (2007) 8957–8970.
[11C] P. Baum, D.-S. Yang, A.H. Zewail, 4D visualization of transitional structures in phase transformations by electron diffraction, Science 318 (2007) 788–792.
[12C] F. Carbone, P. Baum, P. Rudolf, A.H. Zewail, Structural preablation dynamics of graphite observed by ultrafast electron crystallography, Phys. Rev. Lett. 100 (2008) 035501.
[13C] P. Baum, A.H. Zewail, Femtosecond diffraction with chirped electron pulses, Chem. Phys. Lett. 462 (2008) 14–17.
[14C] D.-S. Yang, C. Lao, A.H. Zewail, 4D electron diffraction reveals correlated unidirectional behavior in zinc oxide nanowires, Science 321 (2008) 1660–1664.
[15C] F. Carbone, D.-S. Yang, E. Giannini, A.H. Zewail, Direct role of structural dynamics in electron–lattice coupling of superconducting cuprates, Proc. Natl. Acad. Sci. USA 105 (2008) 20161–20166.
[16C] D.-S. Yang, A.H. Zewail, Ordered water structure at hydrophobic graphite interfaces observed by 4D, ultrafast electron crystallography, Proc. Natl. Acad. Sci. USA 106 (2009) 4122–4126.
[17C] S. Schäfer, W. Liang, A.H. Zewail, Structural dynamics and transient electric-field effects in ultrafast electron diffraction from surfaces, Chem. Phys. Lett. 493 (2010) 11–18.
[18C] S. Schäfer, W. Liang, A.H. Zewail, Primary structural dynamics in graphite, New J. Phys. 13 (2011) 063030.
[19C] S. Schäfer, W. Liang, A.H. Zewail, Structural dynamics of nanoscale gold by ultrafast electron crystallography, Chem. Phys. Lett. 515 (2011) 278–282.
[20C] S. Schäfer, W. Liang, A.H. Zewail, Structural dynamics of surfaces by ultrafast electron crystallography: Experimental and multiple scattering theory, J. Chem. Phys. 135 (2011) 214201.
[21C] W. Liang, S. Schäfer, A.H. Zewail, Ultrafast electron crystallography of monolayer adsorbates on clean surfaces: Structural dynamic, Chem. Phys. Lett. 542 (2012) 1–7.
[22C] W. Liang, S. Schäfer, A.H. Zewail, Ultrafast electron crystallography of heterogeneous structures: Gold-graphene bilayer and ligand-encapsulated nanogold on graphene, Chem. Phys. Lett. 542 (2012) 8–12.

Ultrafast Electron Microscopy (UEM)

[1M] V.A. Lobastov, R. Srinivasan, A.H. Zewail, Four-dimensional ultrafast electron microscopy, Proc. Natl. Acad. Sci. USA 102 (2005) 7069–7073.
[2M] P. Baum, A.H. Zewail, Breaking resolution limits in ultrafast electron diffraction and microscopy, Proc. Natl. Acad. Sci. USA 103 (2006) 16105–16110.

[3M] M.S. Grinolds, V.A. Lobastov, J. Weissenrieder, A.H. Zewail, Four-dimensional ultrafast electron microscopy of phase transitions, Proc. Natl. Acad. Sci. USA 103 (2006) 18427–18431.
[4M] H.S. Park, et al., Atomic-scale imaging in real and energy space developed in ultrafast electron microscopy, Nano Lett. 7 (2007) 2545–2551.
[5M] V.A. Lobastov, J. Weissenrieder, J. Tang, A.H. Zewail, Ultrafast electron microscopy (UEM): Four-dimensional imaging and diffraction of nanostructures during phase transitions, Nano Lett. 7 (2007) 2552–2558.
[6M] D.J. Flannigan, V.A. Lobastov, A.H. Zewail, Controlled nanoscale mechanical phenomena discovered with ultrafast electron microscopy, Angew. Chem., Int. Ed. Engl. 46 (2007) 9206–9210.
[7M] P. Baum, A.H. Zewail, Attosecond electron pulses for 4D diffraction and microscopy, Proc. Natl. Acad. Sci. USA 104 (2007) 18409–18414.
[8M] A. Gahlmann, S.T. Park, A.H. Zewail, Ultrafast electron pulses for diffraction, crystallography, and microscopy: Theoretical and experimental resolutions, Phys. Chem. Chem. Phys. 10 (2008) 2894–2909.
[9M] O.-H. Kwon, et al., 4D visualization of embryonic, structural crystallization by single-pulse microscopy, Proc. Natl. Acad. Sci. USA 104 (2007) 18409–18414.
[10M] B. Barwick, et al., 4D imaging of transient structures and morphologies in ultrafast electron microscopy, Science 322 (2008) 1227–1231.
[11M] O.-H. Kwon, et al., Nanoscale mechanical drumming visualized by 4D electron microscopy, Nano Lett. 8 (2008) 3557–3562.
[12M] F. Carbone, et al., EELS femtosecond resolved in 4D ultrafast electron microscopy, Chem. Phys. Lett. 468 (2009) 107–111.
[13M] D.J. Flannigan, P.C. Samartzis, A. Yurtsever, A.H. Zewail, Nanomechanical motions of cantilevers: Direct imaging in real space and time with 4D electron microscopy, Nano Lett. 9 (2009) 875–881.
[14M] F. Carbone, O.-H. Kwon, A.H. Zewail, Dynamics of chemical bonding mapped by energy-resolved 4D electron microscopy, Science 325 (2009) 181–184.
[15M] O.F. Mohammed, P.C. Samartzis, A.H. Zewail, Heating and cooling dynamics of carbon nanotubes observed by temperature-jump spectroscopy and electron microscopy, J. Am. Chem. Soc. 131 (2009) 16010–16011.
[16M] H.S. Park, et al., Direct observation of martensitic phase-transformation dynamics in iron by 4D single-pulse electron microscopy, Nano Lett. 9 (2009) 3954–3962.
[17M] A. Yurtsever, A.H. Zewail, 4D nanoscale diffraction observed by convergent-beam ultrafast electron microscopy, Science 326 (2009) 708–712.
[18M] H.S. Park, et al., 4D ultrafast electron microscopy: Imaging of atomic motions, acoustic resonances, and moiré fringe dynamics, Ultramicroscopy 110 (2009) 7–19.
[19M] B. Barwick, D.J. Flannigan, A.H. Zewail, Photon-induced near-field electron microscopy, Nature 462 (2009) 902–906.
[20M] D.J. Flannigan, A.H. Zewail, Optomechanical and crystallization phenomena visualized with 4D electron microscopy: Interfacial carbon nanotubes on silicon nitride, Nano Lett. 10 (2010) 1892–1899.
[21M] D.J. Flannigan, B. Barwick, A.H. Zewail, Biological imaging with 4D ultrafast electron microscopy, Proc. Natl. Acad. Sci. USA 107 (2010) 9933–9937.
[22M] O.-H. Kwon, A.H. Zewail, 4D electron tomography, Science 328 (2010) 1668–1673.
[23M] O.-H. Kwon, et al., Nonchaotic, nonlinear motion visualized in complex nanostructures by stereographic 4D electron microscopy, Nano Lett. 10 (2010) 3190–3198.
[24M] D.-S. Yang, O.F. Mohammed, A.H. Zewail, Scanning ultrafast electron microscopy, Proc. Natl. Acad. Sci. USA 107 (2010) 14993–14998.
[25M] H.S. Park, J.S. Baskin, A.H. Zewail, 4D Lorentz electron microscopy imaging: Magnetic domain wall nucleation, reversal, and wave velocity, Nano Lett. 10 (2010) 3796–3803.
[26M] D.J. Flannigan, S.T. Park, A.H. Zewail, Nanofriction visualized in space and time by 4D electron microscopy, Nano Lett. 10 (2010) 4767–4773.
[27M] S.T. Park, M.M. Lin, A.H. Zewail, Photon-induced near-field electron microscopy (PINEM): Theoretical and experimental, New J. Phys. 12 (2010) 123028.
[28M] A. Yurtsever, A.H. Zewail, Kikuchi ultrafast nanodiffraction in four-dimensional electron microscopy, Proc. Natl. Acad. Sci. USA 108 (2011) 3152–3156.
[29M] S.T. Park, D.J. Flannigan, A.H. Zewail, Irreversible chemical reactions visualized in space and time with 4D electron microscopy, J. Am. Chem. Soc. 133 (2011) 1730–1733.
[30M] O.-H. Kwon, V. Ortalan, A.H. Zewail, Macromolecular structural dynamics visualized by pulsed dose control in 4D electron microscopy, Proc. Natl. Acad. Sci. USA 108 (2011) 6026–6031.
[31M] J.S. Baskin, H.S. Park, A.H. Zewail, Nanomusical systems visualized and controlled in 4D electron microscopy, Nano Lett. 11 (2011) 2183–2191.
[32M] O.F. Mohammed, D.-S. Yang, S.K. Pal, A.H. Zewail, 4D scanning ultrafast electron microscopy: Visualization of materials surface dynamics, J. Am. Chem. Soc. 133 (2011) 7708–7711.
[33M] V. Ortalan, A.H. Zewail, 4D scanning transmission ultrafast electron microscopy: Single particle imaging and spectroscopy, J. Am. Chem. Soc. 133 (2011) 10732–10735.
[34M] S.T. Park, A.H. Zewail, Enhancing image contrast and slicing electron pulses in 4D near-field electron microscopy, Chem. Phys. Lett. 521 (2012) 1–6.
[35M] A. Yurtsever, R.M. van der Veen, A.H. Zewail, Subparticle ultrafast spectrum imaging in 4D electron microscopy, Science 335 (2012) 59–64.
[36M] S.T. Park, O.H. Kwon, A.H. Zewail, Chirped imaging pulses in four-dimensional electron microscopy: Femtosecond pulsed hole burning, New J. Phys. 14 (2012) 053046.
[37M] S.T. Park, D.J. Flannigan, A.H. Zewail, 4D electron microscopy visualization of anisotropic atomic motions in carbon nanotubes, J. Am. Chem. Soc. 134 (2012) 9146–9149.
[38M] A. Yurtsever, A.H. Zewail, Direct visualization of near-fields in nanoplasmonics and nanophotonics, Nano Lett. 12 (2012) 3334–3338.
[39M] A. Yurtsever, S. Schäfer, A.H. Zewail, Ultrafast Kikuchi diffraction: Nanoscale stress–strain dynamics of wave-guiding structures, Nano Lett. 12 (2012) 3772–3777.
[40M] A. Yurtsever, J.S. Baskin, A.H. Zewail, Entangled nanoparticles: Discovery by visualization in 4D electron microscopy, Nano Lett. 12 (2012) 5027–5032.
[41M] S.T. Park, A.H. Zewail, Relativistic effects in Photon-induced near-field electron microscopy, J. Phys. Chem. A 116 (2012) 11128–11133.
[42M] D.-S. Yang, O.F. Mohammed, A.H. Zewail, Environmental scanning ultrafast electron microscopy: Structural dynamics of solvation at interfaces, Angew. Chem. Int. Ed. 52 (2013) 2897–2901.
[43M] U.J. Lorenz, A.H. Zewail, Biomechanics of DNA structures visualized by 4D electron microscopy, Proc. Natl. Acad. Sci. USA 110 (2013) 2822–2827.
[44M] R.M. van der Veen, O.-H. Kwon, A.M. Tissot, A. Hauser, A.H. Zewail, Single-nanoparticle phase transitions visualized by 4D electron microscopy, Nat. Chem. 5 (2013) 395–402.
[45M] R.M. van der Veen, A. Tissot, A. Hauser, A.H. Zewail, Unusual molecular material formed through irreversible transformation and revealed by 4D electron microscopy, Phys. Chem. Chem. Phys. 15 (2013) 7831–7838.
[46M] S.T. Park, A. Yurtsever, J.S. Baskin, A.H. Zewail, Graphene-layered steps and their fields visualized by 4D electron microscopy, Proc. Natl. Acad. Sci. USA 110 (2013) 9277–9282.
[47M] A.W.P. Fitzpatrick, S.T. Park, A.H. Zewail, Exceptional rigidity and biomechanics of amyloid revealed by 4D electron microscopy, Proc. Natl. Acad. Sci. USA 110 (2013) 10976–10981.
[48M] A.W.P. Fitzpatrick, U.J. Lorenz, G.M. Vanacore, A.H. Zewail, 4D cryo-electron microscopy of proteins, J. Am. Chem. Soc. (2014).